

# Extreme events at the onset of epileptic-like chimeras in small-world networks of FitzHugh-Nagumo neurons

Javier Cubillos Cornejo, Miguel Escobar Mendoza, and Ignacio Bordeu\*

*Departamento de Física, Facultad de Ciencias Físicas y Matemáticas, Universidad de Chile*

In this work, we investigate the dynamics of complex networks of FitzHugh-Nagumo excitable oscillators, focusing on the impact of coupling strength, network size, and randomness on their collective dynamics. Considering Watts-Strogatz small-world network connectivities, the system exhibits three distinct dynamical phases: chaotic, intermittent, and synchronized, with the intermittent phase displaying transient, epileptic-like chimera states. We analyse the transition to synchronisation by means of the master stability function, and show that peaks in the proportion of extreme events of synchronisation, which correlate with the behaviour of the largest Lyapunov exponent of the system, precede the transitions between the distinct dynamical regimes and mark the onset of epileptic-like chimera states. Our findings contribute to a broader understanding of synchronisation in excitable systems real neural networks and offer insights into the conditions that may lead to pathological epileptic-like states. Furthermore, we discuss the potential use of extreme events to study real neural data.

## I. INTRODUCTION

Synchronisation phenomena occur across diverse fields, ranging from physics and chemistry to biology, neuroscience, and even social systems [1–5]. In the brain, coordinated firing of distinct regions of the brain is crucial for effective information processing. However, when dysregulated, synchronized states can lead to pathological conditions such as epileptic seizures (see Fig. 1a), which disrupt normal brain function [6, 7]. Understanding the conditions that give rise to these coherent events, as well as the biological and physical mechanisms that regulate them, is therefore of considerable importance.

The human brain is composed on billions of neurons, which are grouped and compartmentalized. These compartments establish an intricate functional connectome. Each region of the brain may be modelled as a single node, and interactions between regions as edges connecting nodes, such that the whole brain is reduced to a complex network [8–12] (see Fig. 1b), whose topology follows a small-world organization [13].

A paradigmatic model that captures the excitable and oscillatory regimes of neural systems is the FitzHugh-Nagumo (FHN) oscillator [14], which can be obtained as a qualitative reduction of the classical Hodgkin-Huxley model. This model exhibits a wide range of spatio-temporal phenomena, from extreme events on coupled neurons with time delay [15] and the emergence of Turing patterns in a reduced one dimensional coupled model [16], to chimera states in a non-locally coupled ring [17–23] and synchronisation phase transitions [18, 20, 24, 25]. When coupled through a complex network type of connectivity, chimera states have been related to epileptic seizures in the human brain. These states are characterized by a coexistence of coherent and incoherent phases, and the topology of the connectivity network may alter

the duration of the coherent phases [6, 11, 12]. However, how the network properties and coupling strength control the emergence of these states and how the transition towards intermittent states can be predicted remain unclear.

In this work, we study the interaction between FHN oscillators coupled through a Watts-Strogatz (WS) small-world network, which is characterised by a high degree of clustering and small topological distance between nodes. There are several studies suggesting that real brain networks are not homogeneous, and may present small-world properties [5, 8, 9, 27]. WS networks are constructed starting from a ring lattice with  $N$  nodes, with each node connected to its  $\langle k \rangle$  nearest neighbours, these connections are *rewired* following a random selection rule with probability  $p$  (see Fig. 1c). In this model, the probability of rewiring a connection  $p$  accounts for the degree of randomness of the network:  $p = 0$  corresponds to a regular ring lattice, and  $p = 1$  corresponds to disordered network with small-world properties [5]. The degree distribution of these networks (see Fig. 1d) is affected by  $p$  [28] and the network size  $N$ , and converges to a distribution peaked at  $\langle k \rangle$  that decays exponentially away from it [28]. We note that this contrasts with power-law like decays of scale-free networks.

Here, we show that the system of networked FHN oscillators has three distinct dynamical phases: a chaotic, an intermittent and a synchronised phase. The intermittent phase exhibits transient highly coherent, chimera states separated in time by chaotic behaviour, which were previously related to epileptic-like events [11]. We find that the network size and the level of randomness of its connectivity, as well as the coupling strength between oscillators control the emergence of epileptic-like chimera states. In particular, the network randomness controls the size of the region in the parameter space where epileptic-like events exist and are stable. By computing the master stability function (MSF) of the system, we characterise the transition from intermittency to syn-

\* ibordeu@uchile.cl

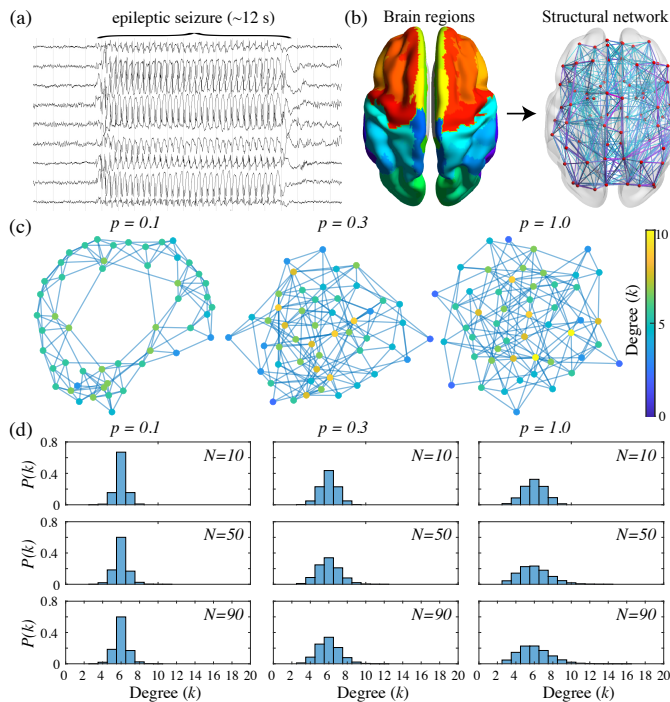


FIG. 1. **Networks of excitable systems.** (a) Electroencephalogram (EEG) from a human brain exhibits synchronised regular activity between distinct regions of the brain, characteristic of an epileptic event (adapted from [26]). (b) Anatomical regions of the brain (left). Regions are interpreted as nodes, and the connectivity network (right) is inferred from the neural activity (adapted from [13]). (c) WS networks for different values of the rewiring probability ( $p$ ), colour of the nodes indicate their degree ( $k$ ). (d) Degree distribution for WS networks for different values of  $p$  (increasing from left to right), and different network sizes (increasing from top to bottom).

chronisation. Furthermore, by analysing the existence of extreme events in the time series of the Kuramoto global order parameter, we show that both the emergence of chimeras and the change in stability of the synchronised manifold are marked by an increase in the probability to observe short transients of anomalous high synchronisation, and we relate these to changes in the values of the largest Lyapunov exponent and dimension of the strange attractor.

The paper is organised as follows: In Sec. IA, we introduce the model, in Sec. IIA, we show that the frequency and duration of epileptic-like events depend on coupling strength, the number of oscillators, and network randomness. In Sec. IIB, we study the dynamical regimes in parameter space, as well as the stability of the synchronous solution. In Sec. IIC, we show that the transitions between dynamical regimes can be characterized by the likelihood of observing extreme synchronisation events. Finally, in Sec. III, we summarise and discuss our results, and their relevance to biological systems.

## A. The model

The FitzHugh-Nagumo model, originally introduced by FitzHugh as a modification of the Van der Pol oscillator and later demonstrated by Nagumo to be analogous to an electrical circuit [29, 30], serves as a well-established framework for modelling excitable systems. The model comprises two variables: an activation variable,  $x(t)$ , which captures the rapid dynamics of excitation, and an inhibition variable,  $y(t)$ , representing the slower recovery process that relaxes the activity back to its basal level. In this study, we consider a network of  $N$  coupled FHN oscillators, where the dynamics of each oscillator is governed by [21, 22, 31, 32]

$$\begin{pmatrix} \varepsilon \dot{x}_i \\ \dot{y}_i \end{pmatrix} = \begin{pmatrix} x_i - \frac{x_i^3}{3} - y_i \\ x_i + a \end{pmatrix} + d \sum_{j=1}^N A_{ij}^p \mathbf{R} \begin{pmatrix} x_j - x_i \\ y_j - y_i \end{pmatrix}, \quad (1)$$

where  $\dot{x}$  and  $\dot{y}$  correspond to the time-derivatives of  $x$  and  $y$ , respectively, and the time-scale separation  $\varepsilon = 0.05$  is fixed so that  $x(t)$  has a fast dynamics compared to  $y(t)$ . The parameter  $a$  controls a transition from an excitable ( $|a| > 1$ ) to an oscillatory ( $|a| < 1$ ) regime. As our interest is to study interactions of actively firing circuits, we set  $a = 0.5$ . The sum term in Eq. (1) accounts for the inter-oscillator coupling, which is proportional to a uniform coupling strength  $d$ . The coupling matrix  $\mathbf{R}$  is defined as

$$\mathbf{R} = \begin{pmatrix} \cos \theta & \sin \theta \\ -\sin \theta & \cos \theta \end{pmatrix}, \quad (2)$$

and controls the level of direct (diagonal) and cross-coupling (off-diagonal terms). We consider  $\theta = \pi/2 - 0.1$ , as values of  $\theta$  close to  $\pi/2$  have been shown to promote the existence of chimera states [22]. The small-world connectivity network is characterised by its  $p$ -dependant adjacency matrix  $A^p$ , whose elements satisfy  $A_{ij}^p = \delta_{ij} k_i - \mathcal{L}_{ij}^p$ , with  $\delta_{ij}$  the Kroenecker delta,  $k_i$  the degree (or number of connections) of the  $i$ th node, and  $\mathcal{L}_{ij}^p$  the element  $(i, j)$  of the Laplacian matrix of the network. Here we consider undirected small-world networks, so that the adjacency matrix is symmetric, and networks are constructed according to the Watts-Strogatz (WS) algorithm with rewiring probability  $p$  and average degree  $\langle k \rangle = 6$  [33]. The results presented here remain mostly unchanged for different choices of  $\langle k \rangle$ .

## B. Kuramoto order parameter

Throughout this work, in order to characterise the synchronicity of the system, we compute the Kuramoto global order parameter [2]

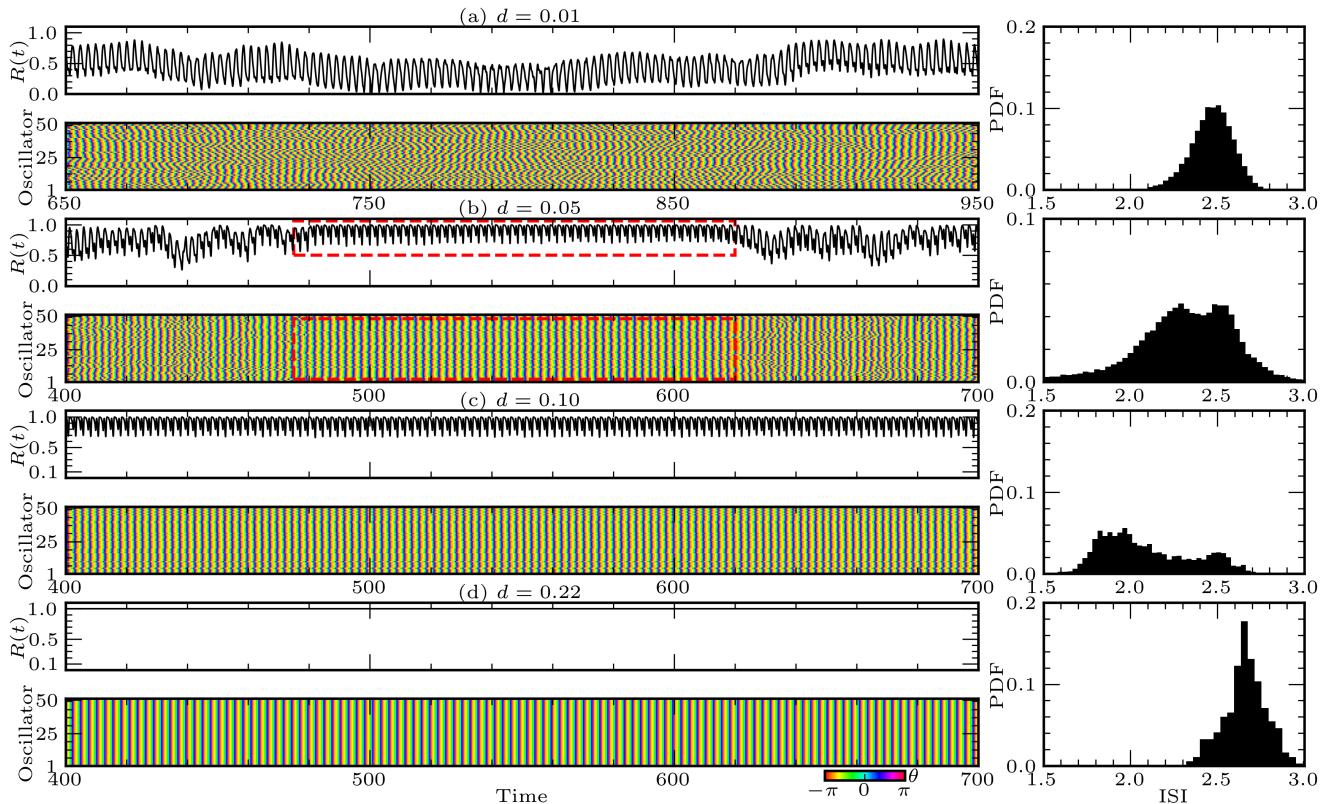


FIG. 2. **Dynamical regimes in networks of FHN oscillators.** Left panels show the time series of the Kuramoto order parameter  $R(t)$  (top), and the temporal evolution of the phases  $\theta_j(t) \in [-\pi, \pi]$  for each of the  $j = 1, \dots, N = 50$  oscillators (bottom), right panels show the distribution of inter-spike intervals (ISI) for the  $N = 50$  oscillators, for coupling (a)  $d = 0.01$  (b)  $d = 0.05$  (c)  $d = 0.10$  (d)  $d = 0.22$ . An epileptic-like event is highlighted in the left panels of (b).

## II. RESULTS

Networks of FHN oscillators exhibit various dynamical regimes, including chaotic (Fig. 2a), intermittent (Fig. 2b), partially and fully synchronised (Fig. 2c and 2d, respectively) states, which depend not only of the strength of the coupling between oscillators ( $d$ ) but also on the system size ( $N$ ) and the network randomness, characterised by the rewiring probability ( $p$ ). By increasing the coupling strength oscillators can alter their firing frequency, transiting from unimodal to bimodal distributions of inter-spike intervals (ISI), up to a threshold value where all oscillators become synchronised in their natural frequency (see right panels in Fig. 2). The bimodal ISI distributions (right panels in Fig. 2b and 2c) result from the existence of chimera states, where coherent and incoherent phases coexist.

### A. Emergence of Epileptic-like events

It has been shown [11] that certain states exhibited by Eq. (1) resemble epileptic-like seizures in the brain, which are characterised by bursts of coherent activity

$$R(t) := \frac{1}{N} \left| \sum_{j=1}^N e^{i\theta_j(t)} \right|, \quad (3)$$

where  $\theta_j(t)$  corresponds to a dynamical phase associated to the fast and slow variables  $x_j(t)$  and  $y_j(t)$  of the oscillator  $j$ , for  $j = \{1, \dots, N\}$  defined as  $\theta_j(t) = \arctan(y_j(t)/x_j(t))$ .  $R(t) \in [0, 1]$ , and gives relevant information about the collective dynamical regimes of the oscillators. Values of  $R \approx 1$  correspond to highly synchronised states, with the limiting value  $R = 1$  accounting for global synchronisation, where  $x_i = x_j$  and  $y_i = y_j$  for all possible values of  $i$  and  $j$ . When  $R \ll 1$  the system is in an incoherent state, where oscillators do not share a common phase.

To study the phase space and the transitions between dynamical regimes as a function of the different parameters, we integrate Eq. (1) numerically (see Appendix A for details) and characterise the parameter space.

separated by periods of incoherent activity (see Fig. 1a and 2b). Here we characterise the region of existence of these epileptic-like events for a range of network sizes,  $N \in [10, 250]$ , rewiring probabilities,  $p \in [0, 1]$ , and coupling strengths,  $d \leq 0$  (Fig. 3).

Similarly to [11], we define an epileptic-like event as a state in which the order parameter  $R(t)$  exceeds a threshold value  $R_{\text{th}} = 0.9$  for period of at least 20 simulation time units. With this, we measured the frequency of epileptic-like events ( $\Omega = \text{number of events/total time}$ ) as a function of the coupling strength and network size for different values of the network rewiring probability,  $p$ , which controls the randomness of the network (see results in Fig. 3a-c).

Our analyses reveal that network randomness is crucial for the emergence of epileptic-like events, which occur only within an intermediate range of coupling strengths (see yellow/red regions in Fig. 3b-c). Interestingly, these events are observed over a broader range of coupling strengths in larger networks, whereas smaller networks tend to exhibit more regular dynamics, limiting the occurrence of such intermittent behaviours. By definition, epileptic-like events correspond to chimera states, whose region of existence lies in the parameter space region limited by fully incoherent chaotic phase (low coupling strength) and a fully synchronised state (high coupling strength).

We note that the duration of these epileptic-like states deep in the intermittence region, followed a power-law like decay, despite of not being in a critical regime (see Fig. 3d). The time between epileptic-like events, on the other hand, followed an exponential decay, with a rate that depended on the parameters  $d$  and  $N$  (see Fig. 3e).

In the following, we study more generally the region of existence of chimeras, and in particular, the transitions between the distinct dynamic regimes.

## B. Characterising the $N$ - $d$ - $p$ phase space

As an initial measure of the collective behaviour of the network of FHN coupled oscillators, we compute the time-averaged global order parameter ( $\bar{R}$ ) as a function of the coupling strength, in a WS networks of different sizes and  $p = 1$  (see Fig. 4a). Here we note that regardless of the network size,  $\bar{R}$  grows monotonically with  $d$ , exhibiting two transitions: One at  $d \sim 0.05$  and another at  $d \sim 0.15$ , after which the system reaches full synchronisation. Notably, in the regions where chimeras are expected (including epileptic-like events) i.e.  $d \sim [0.05, 0.15]$ , the averaged order parameter exhibits a plateau for large-enough system sizes.

Decreasing the rewiring probability,  $p$ , of the Watts-Strogatz network causes a significant increase in the coupling threshold at which the oscillators become fully synchronized (see Fig. 4b-c). This was consistent with an increase in the region of observation of epileptic-like events (see Figs. 3b-c), however this comes with a reduction

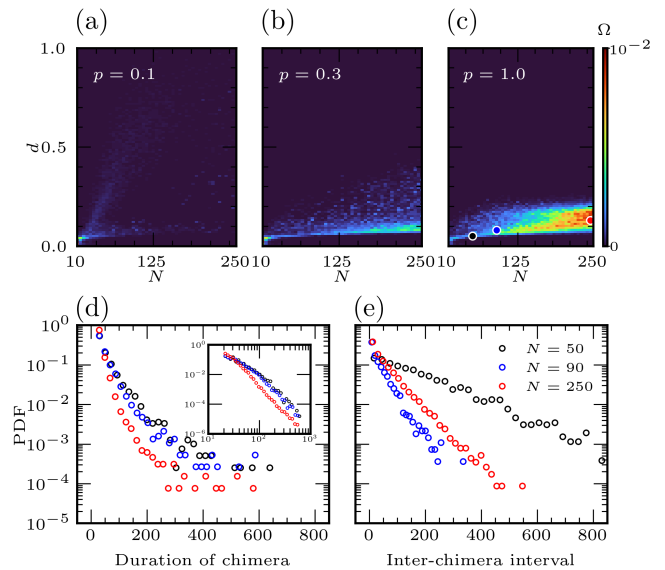


FIG. 3. **Emergence of epileptic-like states.** (a)-(c) Frequency of epileptic-like events in  $(N, d)$ -parameter space, for (a)  $p = 0.1$ , (b)  $p = 0.3$ , and (c)  $p = 1.0$ . (d) Shows the distribution of durations of the epileptic-like events in log-linear and (inset) log-log plots, and (e) shows the distribution of waiting times between epileptic-like events. Time corresponds to arbitrary simulation time units. Circles in panel (c) correspond to the system parameters used for (d) and (e).

in their frequency of appearance. To understand the changes in the transition line to synchronisation we performed a linear stability analysis of the synchronised solution.

### 1. Linear stability analysis of the synchronous solution

A linear stability analysis for the synchronised solution can be achieved by evaluating the Master Stability Function (MSF) of Eq. (1) [3, 34, 35] (see derivation in Appendix B). The MSF is defined as the maximum Lyapunov exponent  $\Lambda_{\text{max}}(\nu)$  associated to the linearised dynamical system describing the time evolution of the perturbations transverse to the synchronous manifold  $\mathcal{S}$ , and allow us to study the stability of  $\mathcal{S}$  as function of a single parameter  $\nu = \gamma_2 d$ , where  $d$  is the coupling strength and  $\gamma_2$  is the second smallest eigenvalue of the network Laplacian matrix, known in the literature as algebraic connectivity [36]. When  $\Lambda_{\text{max}}(\nu) > 0$ ,  $\mathcal{S}$  is unstable, while  $\Lambda_{\text{max}}(\nu) < 0$  provides a necessary condition for the stability of  $\mathcal{S}$  [3]. In Fig. 5a, we show  $\Lambda_{\text{max}}(\nu)$  for  $\alpha = \pi/2 - 0.1$ , which exhibits a positive window for the MSF, and for  $\alpha = 0$ , for which the MSF is always negative and neither chimeras nor incoherent behaviour can be observed.

Consistent with the observations of the time-averaged global order parameter (Fig. 4b-d), lowering the rewiring



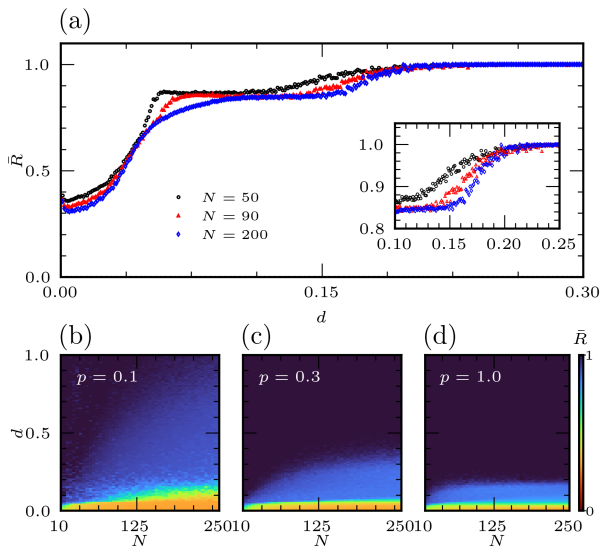


FIG. 4. **Phase transitions of coupled FHN oscillators.** (a) Time-averaged order parameter,  $\bar{R}$ , as a function of the coupling strength,  $d$ , for WS networks with rewiring probability  $p = 1$  and varied sizes,  $N$ . (b)-(d)  $\bar{R}$  in the  $(N, d)$ -parameter space, for (b)  $p = 0.1$ , (c)  $p = 0.3$ , and (d)  $p = 1.0$ .

probability  $p$  causes a shift in the critical curve  $\Lambda_{max}(\nu) = 0$  towards larger values of  $d$  (see Fig. 5b-d). We note that the critical curve was accurately predicted by the Wu-Chua conjecture (see Appendix C), delimiting the region above (below) which the synchronised manifold is stable (unstable), see dashed line in 5b-d.

The MSF analysis shows that the change in the transition line to synchronisation comes from changes in the topological features of the network, which enter in the MSF through the second smallest eigenvalue of the Laplacian matrix of the connectivity network. With this, we have been able to characterize the transition from intermittency (where chimeras are observed) to synchronisation, corresponding to the stabilization of the two-dimensional synchronisation manifold.

As seen earlier with chimera states, the system can still approach the synchronisation manifold in regions where it is unstable. In the following, we show that before transitioning from one dynamical regime to the other, the probability that the system exhibits anomalously high levels of synchronisation reaches maximum levels. We use this as means for characterizing the region of existence of chimera states and, thus epileptic-like events.

### C. Extreme events at the onset of phase transitions

By analysing the probability distribution (PDF) for the global order parameter, we studied the likelihood that an event of high synchronisation occurs spontaneously in the system. For this, we use the standard hydrodynamical criterion [37–39]: Given the PDF  $P(A)$  of an

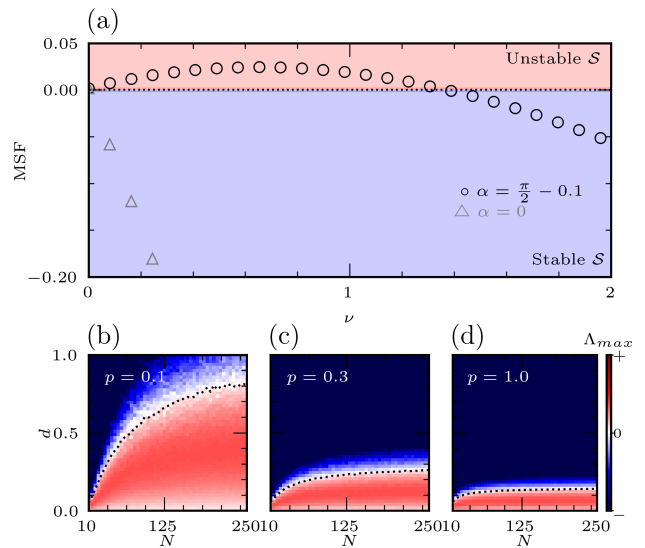


FIG. 5. **MSF of FHN coupled oscillators.** (a)  $\Lambda_{max}(\nu)$ , for  $\alpha = 0$  (grey triangles) and  $\alpha = \pi/2 - 0.1$  (black circles). (b)  $\Lambda_{max}$  for a WS network as a function of the system size,  $N$ , and coupling strength,  $d$ , for rewiring probabilities (b)  $p = 0.1$ , (c)  $p = 0.3$ , and (d)  $p = 1.0$ . The black dashed lines in (b)-(d) show the approximated critical curve,  $\Lambda_{max}(\nu) = 0$ , obtained from the Wu-Chua conjecture (see Appendix C). Shades of red and blue correspond to a positive and negative sign of the MSF, respectively.

observable  $A$ , a value  $y$  of the observable is considered to be extreme if is larger than twice a threshold  $A_s$ , defined as the mean value of the highest tertile of  $P(A)$ , i.e., events with an abnormality index  $I \equiv A/A_s > 2$  (see Fig. 6a). To apply this criterion, we considered the observable  $A(t) = -\log(1 - R(t))$ , which maps the domain of  $R(t)$  from  $[0, 1]$  to  $[0, +\infty)$ . This ensures that the AI is always contained in the domain.

Throughout this section, we refer to  $A$  as *synchronisation amplitude*, and the proportion of extreme events in a time series  $A(t)$  is then defined as

$$p_{EE} = \int_{2A_s}^{\infty} P(A) dA. \quad (4)$$

To illustrate how  $p_{EE}$  changes with the coupling strength, we consider a system of  $N = 50$  oscillators in a WS network with  $p = 1$ . As the coupling strength  $d$  is increased (see Figs. 6b-c), the distribution  $P(A)$  is altered significantly. The distribution transitions from a regime where extreme events of synchronisation amplitude are present (Figs. 6b and d), to a region where no extreme events are observed (see Fig. 6c).

A systematic analysis of the proportion of extreme events revealed a non-monotonic behaviour of  $p_{EE}$  as the coupling strength is increased from zero up to the region of full synchronisation, as shown in Fig. 7a for  $N = 50$  and  $p = 1$ . For low couplings ( $d < 0.05$ ) the  $p_{EE}$  is always

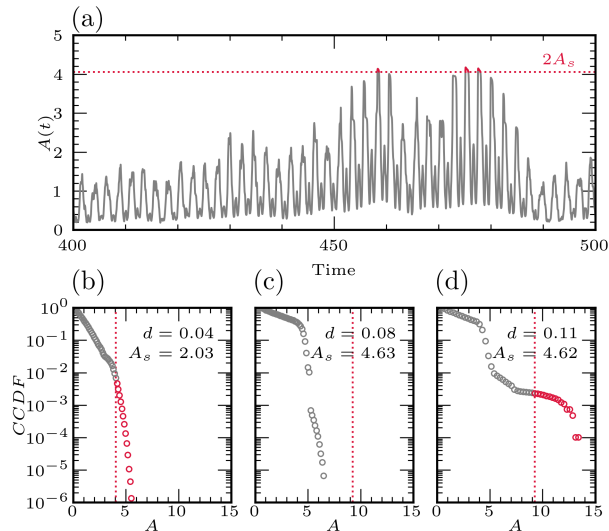


FIG. 6. **Extreme events on networks of FHN oscillators.** (a) Time-series of synchronisation amplitude  $A(t)$ , for  $N = 50$  oscillators,  $d = 0.04$  and  $p = 1.0$ . The dotted line show the value  $2A_s$  above which the values of  $A(t)$  are considered extreme events (shown in red). (b)-(d) Complementary cumulative distributions of  $A$ , for (b)  $d = 0.04$ , (c)  $d = 0.08$ , and (d)  $d = 0.11$ . The vertical dotted lines show the value  $2A_s$ .

positive, showing a peak of events prior to the transition to a region where no extreme events are observed. As  $d$  is increased further, a second peak in the  $p_{EE}$  is observed (for  $d \approx 0.11$ ), above which the  $p_{EE}$  again falls to zero, and remains at zero for all larger values of  $d$ .

To understand this behaviour is worth looking at the nature of the incoherent behaviour for values of  $d$  below the synchronisation transition (as given by the MSF analysis in Fig. 5a). For this, we computed the complete set of  $2N$  Lyapunov exponents  $\{\lambda_i\}_{i=1}^{2N}$  for the system with  $N = 50$  and  $p = 1$ , for all values of  $d$  [35, 40, 41]. The maximum Lyapunov exponent  $\lambda_0$  as a function of  $d$  is shown in Fig. 7b. Moreover, we computed the Kaplan-Yorke dimension, corresponding to an upper bound to the dimension of the strange attractor, which is defined as [35, 41]

$$D_{KY} = j + \sum_{i=1}^j \frac{\lambda_i}{|\lambda_{j+1}|}, \quad (5)$$

where  $j$  is the largest index such that  $\sum_{i=1}^j \lambda_i \geq 0$ . This analysis shows that, as expected, the complete region of incoherence corresponds to a chaotic region, due to the positivity of its largest Lyapunov exponent. In addition, we observe that the peaks in the  $p_{EE}$  as  $d$  is increased, precedes sharp decrease in the Kaplan-Yorke dimension, as has been observed for similar measures in other systems [39]. For the system with  $N = 50$  oscillators, the

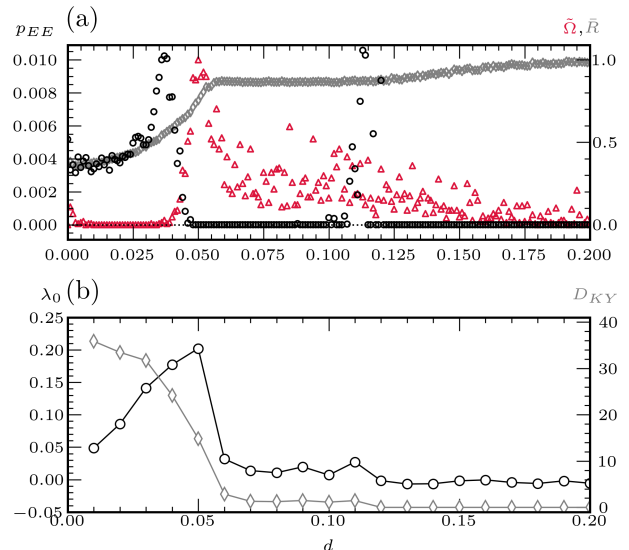


FIG. 7. **Chaos analysis of coupled FHN oscillators.** (a) Left axis: Proportion of extreme events (black circles) for different values of coupling strength  $d$ . Right axis: Frequency of epileptic-like events (red triangles), and order parameter (grey diamonds) as in Fig. 4a. (b) Left axis: Maximum Lyapunov exponent (black circles), right axis: Kaplan-Yorke dimension (grey diamonds). All data shown were obtained from considering a system of  $N = 50$  FHN oscillators on WS networks with  $p = 1.0$ .

first region of positive  $p_{EE}$  ( $d < 0.05$ ) correspond to high-dimensional chaos (see  $D_{KY}$  in Fig. 7b), with the magnitude of the largest Lyapunov exponents increasing with  $d$  before suffering a drastic reduction, just as the peak in the  $p_{EE}$  is passed (see  $\lambda_0$  in Fig. 7b). Interestingly, the peak in  $p_{EE}$  marks the onset for the appearance of epileptic-like events (see Fig. 7a). In the intermediate region, where  $p_{EE} = 0$  ( $0.05 < d < 0.1$ ), the chaotic attractor is significantly contracted and low-dimensional chaos is observed, i.e. there is only one positive Lyapunov exponent. There, the system exhibits coexistence of coherent and incoherent phases and, thus chimeras and epileptic-like events are observed throughout (see Fig. 7a). The second peak in the  $p_{EE}$ , coincides with the critical curve ( $\Lambda_{max} = 0$ ) predicted by the MSF analysis (see Fig. 5d). In this transition, both the largest Lyapunov exponents and the Kaplan-Yorke dimension are further reduced, with  $D_{KY}$  decrease to zero, indicating the stabilization of the synchronisation manifold.

Overall, comparing the time-averaged global order parameter, the frequency of epileptic-like events, the Kaplan-Yorke dimension, and the proportion of extreme events (Figs. 7a-b), we observe that changes in  $D_{KY}$ , as well as the disappearance and appearance of EEs, is directly correlated with the critical values of  $d$  where the transitions occur.

As such, we computed the  $p_{EE}$  in the complete  $N - d$  parameter space (see Fig. 8). Overlaying to this the tran-

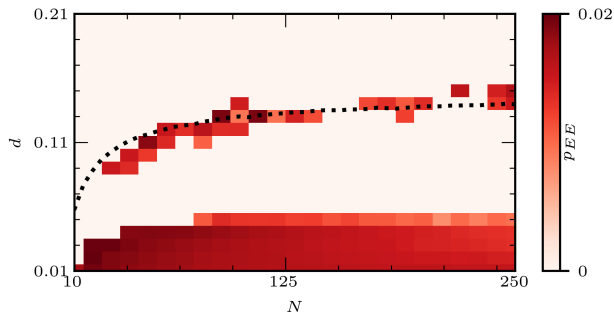


FIG. 8. **Extreme events on WS networks of FHN oscillators.** Proportion of extreme events,  $p_{EE}$ , as a function of the system size ( $N$ ) and coupling strength  $d$ , for  $p = 1.0$ . Pale colour indicates regions where  $p_{EE} = 0$ . The dashed line shows the critical curve where the MSF changes sign, obtained through the Wu-Chua conjecture.

sition curve obtained from the MSF, we observe that peaks in the proportion of extreme events accurately predict the transition to the synchronised phase. Comparing with the frequency of epileptic-like events, we observe that their appearance is preceded by a peak in  $p_{EE}$ , and their frequency is maximum in the intermediate region where  $p_{EE} = 0$ .

### III. CONCLUSIONS AND DISCUSSION

In this study, we explored the dynamics of coupled FitzHugh-Nagumo oscillators on Watts-Strogatz small-world networks. Our results show that network randomness and coupling strength significantly influence the occurrence of epileptic-like states, which resemble the transient synchronisation observed in real neural networks during seizures.

Interestingly, epileptic-like events occur only within an intermediate range of coupling strengths and become more frequent as the network becomes larger provided that the rewiring probability is large enough (as was shown in Fig. 3b-c). This opens questions about the compartmentalization in animal brains, and the mechanisms of wiring in healthy and altered conditions. In humans, for instance, anatomical inspection of the brain allows to identify of the order of 90 distinct regions [42, 43], with an inhomogeneous (small-world-like) structural connectivity (see Fig. 1b). According to our theoretical observations, this brain organisation promotes the coexistence between coherent and incoherent phases, yet it remains unclear what are the mechanisms that lead to this organisation.

Evaluating the master stability function allowed us to find the transition curve to synchronisation in the  $N - d$  parameter spaces for different values of the rewiring probability. This curve separated the phase space into a synchronised and a chaotic phase, as demonstrates by the Lyapunov exponent analysis. Within the chaotic phase,

we distinguished two regions, which became apparent with when analysing the proportion of extreme events in the (rescaled) order parameter: A fully chaotic region and a region of coexistence between an incoherent and a coherent phase, where chimera states and epileptic-like events were observed. We have shown that the transitions from chaos to intermittency, and subsequently to synchronisation, are preceded by rise in the frequency of synchronisation events, a behaviour that correlates with significant changes in the dimensionality of the system's strange attractor.

We note that experimentally, the computation of the Lyapunov exponents is challenging. However, computing the proportion of extreme events  $p_{EE}$  requires only a sufficiently long time series in order to construct the PDF of a relevant observable, which may provide useful information of the distinct dynamical phases of the system. This type of characterization of the phase space could open the door for the potential analysis of real EEG data or larger system sizes, where access to the Lyapunov spectrum may be limited, but long time series of the neural dynamic are more readily available.

In conclusion, this work contributes to a deeper understanding of the interplay between network structure, coupling strength, and neural dynamics. The findings may have broader implications for understanding neural processes, offering potential applications in modelling the conditions that lead to pathological states such as epilepsy. Future work could extend this analysis to dynamical network topologies and explore the effects of additional biological factors, such as noise and time delays, to better model realistic neural systems.

### ACKNOWLEDGMENTS

I.B. acknowledges the financial support from FONDECYT grant 11230941, and Universidad de Chile-VID grant UI-015/22. The authors wish to thank Magdalena Sanhueza, Claudio Falc3n, Karin Alfaro-Bittner and Marcel Clerc for useful discussions.

### Appendix A: Numerical simulations

The dynamics of coupled FHN oscillators are solved by integrating Eq. (1) with a fourth-order Runge-Kutta method, considering random initial conditions following a uniform distribution  $x \sim U_x(-a, a)$ ,  $y \sim U_y(-a + a^3/3, a + a^3/3)$  and a suitable time step that ensures convergence. Specifically, simulations in (Fig. 2) consider the time evolution of  $1 \times 10^4$  steps, and the ISI PDF is calculated after a transient of  $1 \times 10^2$  time steps. Simulations in (Fig. 3a-e, 4a-d and 7a) consider the time evolution of  $1 \times 10^5$  time steps. The computation of  $\Omega$  for each point in the  $N - d - p$  space in (Fig. 3a-c) is calculated by averaging the analysis of 50 realisations of  $R(t)$ , excluding the final  $1 \times 10^3$  time steps, in order to consider only

epileptic-like events. Additionally, distributions in (Fig. 3d-e) are calculated based on the analysis of 1500 realisations of  $R(t)$ , for each system size and coupling strength indicated. The time-averaged global order parameter  $\bar{R}$  in (Fig. 4a-d, 7a) is calculated as a long-time average of  $5 \times 10^4$  time steps after a sufficiently large transient of  $5 \times 10^4$  time steps has elapsed, averaged over 50 realisations. The proportion of extreme events  $p_{EE}$  in (Fig. 7a) is calculated through the analysis of 50 realisations of  $A(R(t))$ . Simulations in (Fig. 6a-d and 8) consider the time evolution of  $1 \times 10^6$  time steps, and both the distributions and  $p_{EE}$  are calculated considering 50 realisations of  $A(R(t))$ . Finally, the dynamical systems involved in the algorithms for computing the Lyapunov exponents [35, 40, 41] were solved with a fourth-order Runge-Kutta method for  $1 \times 10^3$  time units with an adaptive time step and suitable parameters that ensure convergence.

### Appendix B: Master Stability Function

To perform a linear stability analysis in order to understand the transition to synchronisation, we study the MSF for the system of Eq. (1) as in [3, 44]. Let  $(x_S, y_S)^T \in \mathcal{S}$ , whose orbits obeys:

$$\begin{aligned} \varepsilon \dot{x}_S(t) &= f(x_S, y_S) = x_S - \frac{x_S^3}{3} - y_S \\ \dot{y}_S(t) &= g(x_S, y_S) = x_S + a. \end{aligned} \quad (\text{B1})$$

Let  $(\delta x_i, \delta y_i)^T = (x_i(t) - x_S, y_i(t) - y_S)^T$  be small perturbations away from  $\mathcal{S}$ . Consider now the relation  $A_{ij}^p = \delta_{ij} k_i - \mathcal{L}_{ij}^p$ , where  $\delta_{ij}$  is the Kronecker delta,  $k_i$  is the degree of the  $i$  node,  $p$  is the rewiring probability of the Watts-Strogatz model and  $A_{ij}^p, \mathcal{L}_{ij}^p$  are the elements of the adjacency and Laplacian matrix of the network  $A^p$  and  $\mathcal{L}^p$ , respectively. Linearising around  $(x_S, y_S)^T$ , and using the property  $\sum_j \mathcal{L}_{ij}^p = 0$ , the perturbations evolves as

$$\begin{aligned} \delta \dot{x}_i &= \frac{(1 - x_S^2)}{\varepsilon} \delta x_i + \frac{\delta y_i}{\varepsilon} - d \sum_{j=1}^N \mathcal{L}_{ij}^p \left[ \frac{\cos \alpha}{\varepsilon} \delta x_j + \frac{\sin \alpha}{\varepsilon} \delta y_j \right] \\ \delta \dot{y}_i &= \delta x_i - d \sum_{j=1}^N \mathcal{L}_{ij}^p [-\sin \alpha \delta x_j + \cos \alpha \delta y_j]. \end{aligned} \quad (\text{B2})$$

Let now  $V^p$  be the matrix of eigenvectors of  $\mathcal{L}^p$  and  $\xi_i = (\xi_i^x, \xi_i^y)^T$  the projections of the perturbations on the eigenvector basis

$$\xi_i = (\xi_i^x, \xi_i^y)^T = \left( \sum_{j=1}^N V_{ij}^p \delta x_j, \sum_{j=1}^N V_{ij}^p \delta y_j \right)^T, \quad (\text{B3})$$

which corresponds to the decoupled eigenmodes identified by the eigenvectors of  $\mathcal{L}^p$  with associated eigenvalues  $\gamma_1^p < \gamma_2^p < \dots < \gamma_i^p < \dots < \gamma_N^p$ , thus the relation  $\mathcal{L}_{kj}^p V_{ij}^p = \delta_{kj} V_{ij}^p \gamma_i^p$  holds. Using this, Eq. (B2) becomes

$$\begin{aligned} \dot{\xi}_i^x &= \frac{(1 - x_S^2)}{\varepsilon} \xi_i^x - \frac{\xi_i^y}{\varepsilon} - \gamma_i^p d \left[ \frac{\cos \alpha}{\varepsilon} \xi_i^x + \frac{\sin \alpha}{\varepsilon} \xi_i^y \right] \\ \dot{\xi}_i^y &= \xi_i^x - \gamma_i^p d [-\sin \alpha \xi_i^x + \cos \alpha \xi_i^y]. \end{aligned} \quad (\text{B4})$$

The equations above can be written as

$$\dot{\xi}_i = \mathbf{K}(\nu_i) \xi_i, \quad (\text{B5})$$

where  $\nu_i = \gamma_i^p d$ , and

$$\mathbf{K}(\nu_i) = \begin{pmatrix} (1 - x_S^2 - \nu_i \cos \alpha)/\varepsilon & -1 - \nu_i \sin \alpha \\ (1 + \nu_i \sin \alpha)/\varepsilon & -\nu_i \cos \alpha \end{pmatrix}, \quad (\text{B6})$$

letting  $\nu_i$  be an arbitrary value  $\nu$ , we arrive to

$$\dot{\xi} = \mathbf{K}(\nu) \xi. \quad (\text{B7})$$

We compute the MSF of the system which correspond to the maximum Lyapunov exponent  $\Lambda_{max}$  of Eq. (B7) via the standard procedure developed in [35, 41] for suitable parameters that ensure the convergence of the algorithm.

### Appendix C: The Wu-Chua conjecture

To quantify and understand in a more detailed manner the stability regions of the synchronisation manifold in the parameter space  $N - d$ , we test the Wu-Chua conjecture [45], which gives a relation between the second smallest eigenvalue of the Laplacian matrix of a graph and the critical coupling strength needed for synchronisation of two different systems. Let  $(s.i)$  and  $(s.ii)$  be two linearly coupled systems with  $N_1$  and  $N_2$  units with respective laplacian matrices  $\mathcal{L}_1$  and  $\mathcal{L}_2$  whose smallest eigenvalues are  $\gamma_2(N_1)$  and  $\gamma_2(N_2)$ , then the following relation holds:

$$d_{N_1}^c = \frac{d_{N_2}^c \gamma_2(N_2)}{\gamma_2(N_1)}, \quad (\text{C1})$$

where  $d_{N_1}^c$  and  $d_{N_2}^c$  correspond to the critical coupling strength for synchronisation for  $(s.i)$  and  $(s.ii)$ , respectively. We consider the system  $(s.i)$  and  $(s.ii)$  both to be FitzHugh-Nagumo coupled oscillators whose dynamics obeys Eq. (1). In this case,  $(s.i)$  corresponds to the system of  $N$  units interacting over a Watts-Strogatz network of the model described in Sec. I with Laplacian matrix  $\mathcal{L}_{ij}^p$ , whose second smallest eigenvalue  $\gamma_2(N; p, \langle k \rangle)$  is computed numerically, and  $(s.ii)$  corresponds to a



system of  $N_2 = 2$  coupled units whose Laplacian matrix is  $\mathcal{L}_2 = \begin{bmatrix} 1 & -1 \\ -1 & 1 \end{bmatrix}$ , with second smallest eigenvalue  $\gamma_2(N_2) = 2$ . The synchronisation threshold for system (*s.ii*) is obtained via the MSF procedure described in Appendix B, and we find it to be  $d_{N_2}^c \approx 0.105 \approx 1/10$ . The relation (C1) becomes

$$d_{WC}^c(N; p, \langle k \rangle) = \frac{1}{5\gamma_2(N; p, \langle k \rangle)}, \quad (\text{C2})$$

which correspond to the curves shown in Fig. 4b-d and 5b-d, where we have considered  $\langle k \rangle = 6$  according to the WS network studied.

- 
- [1] A. Pikovsky, M. Rosenblum, and J. Kurths, *Synchronization: A Universal Concept in Nonlinear Sciences* (Cambridge University Press, 2003).
- [2] Y. Kuramoto, *Chemical Turbulence* (Springer, 1984).
- [3] S. Boccaletti, A. N. Pisarchik, C. I. Del Genio, and A. Amann, *Synchronization: From Coupled Systems to Complex Networks* (Cambridge University Press, 2018).
- [4] G. Pruessner, *Self-Organised Criticality: Theory, Models and Characterisation* (Cambridge University Press, 2012).
- [5] A.-L. Barabási, *Network Science* (Cambridge University Press, 2016).
- [6] L. G. Sadleir, I. E. Scheffer, S. Smith, B. Carstensen, J. Carlin, M. B. Connolly, and K. Farrell, Factors influencing clinical features of absence seizures, *Epilepsia* **49**, 2100 (2008).
- [7] P. Bonifazi, M. Goldin, M. A. Picardo, I. Jorquera, A. Cattani, G. Bianconi, A. Represa, Y. Ben-Ari, and R. Cossart, Gabaergic hub neurons orchestrate synchrony in developing hippocampal networks, *Science* **326**, 1419 (2009).
- [8] E. Bullmore and O. Sporns, Complex brain networks: Graph theoretical analysis of structural and functional systems, *Nat. Rev. Neurosci.* **10**, 186 (2009).
- [9] X. Li, G. Ouyang, A. Usami, Y. Ikegaya, and A. Sik, Scale-free topology of the ca3 hippocampal network: A novel method to analyze functional neuronal assemblies, *Biophys. J.* **98**, 1733 (2010).
- [10] M. Breakspear, S. Heitmann, and A. Daffertshofer, Generative models of cortical oscillations: Neurobiological implications of the kuramoto model, *Front. Hum. Neurosci.* **4**, 190 (2010).
- [11] M. Gerster, R. Berner, J. Sawicki, A. Zakharova, A. Škoch, J. Hlinka, K. Lehnertz, and E. Schöll, Fitzhugh-nagumo oscillators on complex networks mimic epileptic-seizure-related synchronization phenomena, *Chaos* **30**, 123130 (2020).
- [12] J. Sawicki and E. Schöll, Interplay of synchronization and cortical input in models of brain networks, *EPL* **146**, 41001 (2024).
- [13] Y. Sun, R. Lee, Y. Chen, S. Collinson, N. Thakor, A. Bezzerianos, and K. Sim, Progressive gender differences of structural brain networks in healthy adults: A longitudinal, diffusion tensor imaging study, *PLoS ONE*. **10**, e0118857 (2015).
- [14] D. Cebrián-Lacasa, P. Parra-Rivas, D. Ruiz-Reynés, and L. Gelens, Six decades of the fitzhugh-nagumo model: A guide through its spatio-temporal dynamics and influence across disciplines (2024), arXiv:2404.11403.
- [15] A. Saha and U. Feudel, Extreme events in fitzhugh-nagumo oscillators coupled with two time delays, *Phys. Rev. E*. **95**, 062219 (2017).
- [16] T. Carletti and H. Nakao, Turing patterns in a network-reduced fitzhugh-nagumo model, *Phys. Rev. E*. **101**, 022203 (2020).
- [17] A. Rontogiannis and A. Provata, Chimera states in fitzhugh-nagumo networks with reflecting connectivity, *Eur. Phys. J. B* **94**, 97 (2021).
- [18] E. Schöll, Synchronization patterns and chimera states in complex networks: Interplay of topology and dynamics, *Eur. Phys. J. Spec. Top.* **225**, 891 (2016).
- [19] T. Makinwa, K. Inaba, T. Inagaki, Y. Yamada, T. Leleu, T. Honjo, T. Ikuta, K. Enbutsu, T. Umeki, R. Kasahara, *et al.*, Experimental observation of chimera states in spiking neural networks based on degenerate optical parametric oscillators, *Commun. Phys.* **6**, 121 (2023).
- [20] T. Chouzouris, I. Omelchenko, A. Zakharova, J. Hlinka, P. Jiruska, and E. Schöll, Chimera states in brain networks: Empirical neural vs. modular fractal connectivity, *Chaos* **28**, 045112 (2018).
- [21] I. Omelchenko, A. Provata, J. Hizanidis, E. Schöll, and P. Hövel, Robustness of chimera states for coupled fitzhugh-nagumo oscillators, *Phys. Rev. E*. **91**, 022917 (2015).
- [22] I. Omelchenko, O. E. Omel'chenko, P. Hövel, and E. Schöll, When nonlocal coupling between oscillators becomes stronger: Patched synchrony or multichimera states, *Phys. Rev. Lett.* **110**, 224101 (2013).
- [23] A. Zakharova, *Chimera Patterns in Networks* (Springer, 2020).
- [24] N. Semenova, A. Zakharova, V. Anishchenko, and E. Schöll, Coherence-resonance chimeras in a network of excitable elements, *Phys. Rev. Lett.* **117**, 014102 (2016).
- [25] T. Yanagita, T. Ichinomiya, and Y. Oyama, Pair of excitable fitzhugh-nagumo elements: Synchronization, multistability, and chaos, *Phys. Rev. E*. **72**, 056218 (2005).
- [26] C. Cerminara, A. Coniglio, N. El-Malhany, L. Casarelli, and P. Curatolo, Two epileptic syndromes, one brain: Childhood absence epilepsy and benign childhood epilepsy with centrotemporal spikes, *Seizure* **21**, 70 (2012).
- [27] D. S. Bassett and E. Bullmore, Small-world brain networks, *The Neuroscientist* **12**, 512 (2006).
- [28] A. Barrat and M. Weigt, On the properties of small-world network models, *Eur. Phys. J. B.* **13**, 547 (2000).
- [29] R. FitzHugh, Impulses and physiological states in the-

- oretical models of nerve membrane, *Biophys. J.* **1**, 445 (1961).
- [30] J. Nagumo, S. Arimoto, and S. Yoshizawa, An active pulse transmission line simulating nerve axon, *Proc. IRE.* **50**, 2061 (1962).
- [31] E. Schöll, G. Hiller, P. Hövel, and M. A. Dahlem, Time-delayed feedback in neurosystems, *Philos. Trans. R. Soc. A.* **367**, 1079 (2009).
- [32] S. Brandstetter, M. Dahlem, and E. Schöll, Interplay of time-delayed feedback control and temporally correlated noise in excitable systems, *Philos. Trans. R. Soc. A.* **368**, 391 (2010).
- [33] D. J. Watts and S. H. Strogatz, Collective dynamics of ‘small-world’ networks, *Nature* **393**, 440 (1998).
- [34] L. M. Pecora and T. L. Carroll, Master stability functions for synchronized coupled systems, *Phys. Rev. Lett.* **80**, 2109 (1998).
- [35] A. Pikovsky and A. Politi, *Lyapunov Exponents: A Tool to Explore Complex Dynamics* (Cambridge University Press, 2016).
- [36] F. R. Chung, *Spectral Graph Theory*, Vol. 92 (American Mathematical Soc., 1997).
- [37] C. Kharif, E. Pelinovsky, and A. Slunyaev, *Rogue Waves in the Ocean* (Springer Science & Business Media, 2008).
- [38] F. Selmi, S. Coulibaly, Z. Loghmari, I. Sagnes, G. Beaudoin, M. G. Clerc, and S. Barbay, Spatiotemporal chaos induces extreme events in an extended microcavity laser, *Phys. Rev. Lett.* **116**, 013901 (2016).
- [39] M. G. Clerc, G. González-Cortés, and M. Wilson, Extreme events induced by spatiotemporal chaos in experimental optical patterns, *Opt. Lett.* **41**, 2711 (2016).
- [40] F. Christiansen and H. H. Rugh, Computing lyapunov spectra with continuous gram-schmidt orthonormalization, *Nonlinearity* **10**, 1063 (1997).
- [41] C. Skokos, *The Lyapunov Characteristic Exponents and their Computation* (Springer, 2009) pp. 63–135.
- [42] N. Tzourio-Mazoyer, B. Landeau, D. Papathanassiou, F. Crivello, O. Etard, N. Delcroix, B. Mazoyer, and M. Joliot, Automated anatomical labeling of activations in spm using a macroscopic anatomical parcellation of the mni mri single-subject brain, *Neuroimage* **15**, 273 (2002).
- [43] A. Škoch, B. Reháková, J. Mareš, J. Tintěra, P. Sanda, L. Jajcay, J. Horáček, F. Španiel, and J. Hlinka, Human brain structural connectivity matrices-ready for modelling, *Sci. Data.* **9**, 486 (2022).
- [44] S. Rakshit, B. K. Bera, D. Ghosh, and S. Sinha, Emergence of synchronization and regularity in firing patterns in time-varying neural hypernetworks, *Phys. Rev. E.* **97**, 052304 (2018).
- [45] C. W. Wu and L. O. Chua, On a conjecture regarding the synchronization in an array of linearly coupled dynamical systems, *IEEE Trans. Circuits Syst. I: Fundam. Theory Appl.* **43**, 161 (1996).